An order-disorder phase transition in the van-der-Waals based Solvate of C_{60} and $CClBrH_2$

Jin Ye[a], Maria Barrio [a], René Céolin[a,b], Navid Qureshi[c], Philippe Negrier[d], Ivo B. Rietveld[e,f], Josep Lluís Tamarit[a,*]

The co-crystal of C_{60}·$2CBrClH_2$ possesses a monoclinic (C2/m) structure at room temperature with both molecular entities, C_{60} and $CBrClH_2$, orientationally ordered. At 322 K, it transforms reversibly into a hexagonal (P6/mmm) setting, revealing a rare example of a heteromolecular stator-rotator transition in a fullerene co-crystal, which applies to both the fullerene and the coformer analogous to the paradigmatic C_{60}-cubane co-crystal. However, in the present case, topological molecular surface matching between the two chemical species is not necessary and the order-disorder phase transition reflects a simultaneous activation of the orientational disorder of both C_{60} and $CBrClH_2$.

Introduction

Materials solely consisting of carbon, carbon allotropes, such as fullerenes, carbon nanotubes and graphenes, exhibit extraordinary differences in their properties depending on the synthesis conditions.[1-3] Among these materials, fullerenes are of interest due to their large number of potential applications.[4-7] In particular co-crystals and solvates, formed by intercalation of organic or inorganic molecules or even metals into the fullerene structures, have acquired a renewed interest during the last decade.[8,9] This is because solvates, or more precisely hexagonal close packed solvates, tend to easily form nanowires not only with high conductivity but also with extraordinary mechanical properties, as has been demonstrated by the discovery of incompressible phases, which are harder than diamond at high pressure.[3,8,10] In these systems, the superior mechanical properties are related to the 3D network of covalently bonded C atoms between rigid C_{60} molecules together with dopant molecules acting as a spacer between C_{60} units and as a linker between collapsed C_{60} units.

The more fundamentally interesting rotator-stator co-crystals of C_{60} or C_{70} with cubane (C_8H_8) have been discovered recently.[11,12] The cubic shape and the concave surface of cubane create an almost perfect topological fit with the convex surface of the C_{60} molecules when static (orientationally ordered) cubane molecules occupy octahedral voids of the face-centered-cubic structures of rotating fullerenes. When cooling such co-crystals, a phase transition (around 140 K for co-crystals with C_{60} and 150 K with C_{70}) occurs into an orientationally ordered phase (orthorhombic or tetragonal, respectively). The C_{60}- and C_{70}-cubane co-crystals were reported as the first rotator-stator heteromolecular crystals in which stability is provided due to the perfect match of the molecular surfaces of the involved chemical species.

In this work, we report on C_{60}-$CBrClH_2$ co-crystals. It will be demonstrated that a low-temperature monoclinic C_{60}·$2CBrClH_2$ co-crystal in which both molecular species are orientationally ordered undergoes a phase transition around room temperature to a high-temperature hexagonal phase without change of stoichiometry, in which $CBrClH_2$ molecules occupy the prismatic voids of the hexagonal lattice and both C_{60} and $CBrClH_2$ are orientationally disordered. Its behavior will be compared with the recently studied monoclinic C_{60}·$2CBr_2H_2$ co-crystal[13] in which both molecular species are orientationally ordered. The co-crystal here reported displays a C2/m lattice symmetry and despite the overall packing it is quite similar to the hexagonal packing of solvates formed between C_{60} and halogen-methane derivatives. [14-22]

Experimental

Fullerene C_{60} was purchased from TermUSA (purity higher than 99.98%) whereas bromochloro-methane ($CBrClH_2$) was purchased from Aldrich (purity higher than 99.5%). Co-crystals were prepared at room temperature by mixing C_{60} powder with $CBrClH_2$ liquid. After a few months, the morphology of the fcc C_{60} crystals disappeared and new crystals appeared.

The structure and phase transitions of the C_{60}·$CBrClH_2$ co-crystals were studied by means of X-ray powder diffraction (XRPD), differential scanning calorimetry (DSC) and thermogravimetric analysis (TG). XRPD was conducted by means of a high-resolution horizontally mounted INEL cylindrical position-sensitive detector (CPS-120) using Debye-Scherrer geometry (angular step ca. 0.029°-2θ over a 2θ-range from 2 to 115°) equipped with a monochromatic Cu $K\alpha_1$ (λ

[a] Grup de Caracterització de Materials, Departament de Física, EEBE and Barcelona Research Center in Multiscale Science and Engineering, Universitat Politècnica de Catalunya, Av. Eduard Maristany, 10-14, 08019 Barcelona, Catalonia, Spain.
[b] LETIAM, EA7357, IUT Orsay, Université Paris Sud, rue Noetzlin, 91405 Orsay Cedex, France.
[c] Institut Laue Langevin, 71 avenue des Martyrs - CS 20156 - 38042 GRENOBLE CEDEX 9, France.
[d] LOMA, UMR 5798, CNRS, Université de Bordeaux, F-33400 Talence, France.
[e] Normandie Université, Laboratoire SMS, EA 3233, Université de Rouen, F76821 Mont Saint Aignan, France.
[f] Université Paris Descartes, Faculté de Pharmacie, 4 avenue de l'observatoire, 75006 Paris, France.
E-mail: josep.lluis.tamarit@upc.edu Tel: +34934016564
†Electronic Supplementary Information (ESI) available: [details of any supplementary information available should be included here]. See DOI: 10.1039/x0xx00000x

`

=1.5406 Å) radiation (40 kV and 25 mA). Temperature was controlled with a liquid nitrogen 700 series Cryostream Cooler from Oxford Cryosystems (±0.1 K). Samples were held in a 0.5-mm-diameter Lindemann glass capillary and rotated during data acquisition to minimize the effect of preferential orientation.

Pseudo-Voigt fits of the Bragg peaks were used to determine the peak position and lattice parameters with XCELL. For the disordered structures, Rietveld refinement was carried out with the FullProf Suite[23] while the C_{60} molecule was described with spherical harmonics as a homogeneous distribution of 60 C-atoms positioned on a sphere with a radius of 3.59 Å. For the ordered structures, the Materials Studio[24] package was used. In both cases, the $CBrClH_2$ molecule was described as a rigid body (C-Cl: 1.76 Å, C-Br: 1.93 Å, C-H: 1.09 Å).

DSC measurements were performed on a Q100 analyzer from TA Instruments (New Castle, DE, USA) with masses from 5 to 20 mg and heating rates typically of 2 K min^{-1} in hermetically sealed high-pressure stainless steel pans from Perkin–Elmer to resist the vapor pressures of the solvent. TG experiments were conducted under a nitrogen flow with a Q50 thermobalance from TA Instruments (New Castle, DE, USA) at a 2 K min^{-1} rate with masses ranging between 2 and 10 mg.

Results and discussion

Due to the fast decomposition of the C_{60} – $CBrClH_2$ co-crystals outside of the mother liquor at room temperature, both were introduced into a Lindeman capillary to obtain XRPD patterns at 303 K (Fig. 1).

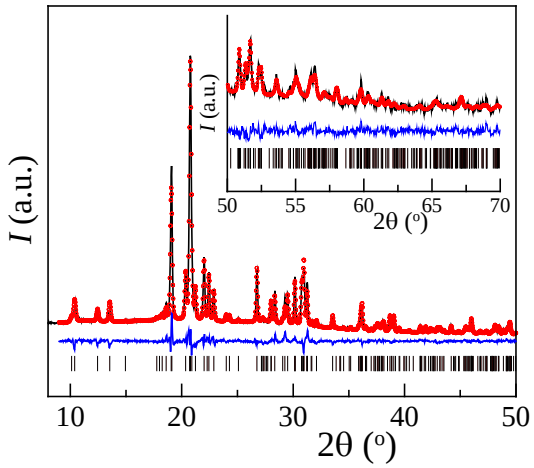

Fig.1. Experimental (red circles) and calculated (black line) X-ray powder diffraction pattern at 303 K along with the difference profile (blue line) and Bragg reflections (vertical bars) of the monoclinic C2/m space-group of the C_{60}·$2CBrClH_2$ co-crystal. The inset provides the data between 50 and 70° (2θ) at increased scale.

The XRPD pattern obtained at 303 K was indexed using XCELL. It resulted in a monoclinic unit cell with lattice parameters (after Rietveld refinement) a = 9.9153(6) Å, b = 17.412(2) Å, c = 10.0478(6) Å, β = 101.966(3)º, V = 1697.0(5) $Å^3$) and the systematic absences are compatible with the space group C2/m (isostructural to the C_{60}·$2CBr_2H_2$ co-crystals).

Monoclinic co-crystals together with a small quantity of the mother liquor were taken from the beaker for TG analyses. The sample mass was in first instance recorded at constant temperature (303 K) leading to the inflection point “a” (in Fig.2) indicating the complete depletion of the mother liquor. The sample mass continued to decrease, while the temperature remained constant, indicating that the co-crystals are unstable under nitrogen gaz. On heating, the sample subsequently lost more mass with a total decrease from the inflection point “a” on of 26%, i.e. close to the 27% calculated for a C_{60} : 2 $CBrClH_2$ molar ratio.

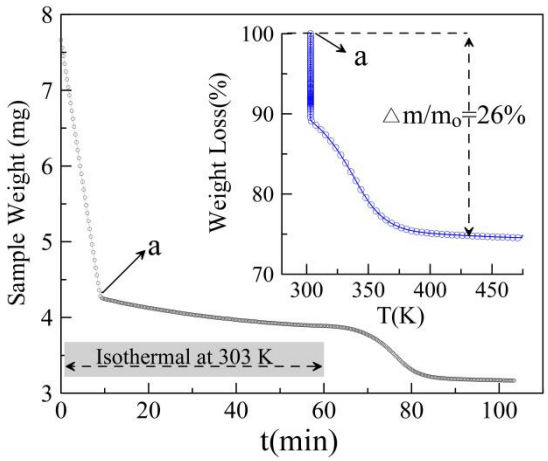

Fig. 2. Thermogravimetric analysis of a heterogeneous sample consisting of C_{60}·$2CBrClH_2$ co-crystals and an excess of mother liquor (vertical axis: sample mass). From t = 0 to t = 60 min at isothermal conditions (303 K) (shaded area) followed by heating with a scanning rate of 5 K·min^{-1}. Evaporation rate: −0.38 mg·min^{-1} in the first part (t = 0 to t = t_a). Inset: detail of the curve following inflection point “a” (mass loss is expressed in % of the weight of the sample defined by point “a”).

With the 1 C_{60} : 2 $CBrClH_2$ stoichiometry, Rietveld refinement was carried out using Materials Studio and applying the rigid-body constraint for $CBrClH_2$, (the molecular structure was based on the data of Podsiadło et al.)[25] The positions and orientations of the molecules were refined with a single overall isotropic displacement parameter and a preferred orientation correction using the March-Dollase formula.[26] The refinement result has been presented in Fig. 1, together with the experimental pattern. Surprisingly, both C_{60} and $CBrClH_2$ are orientationally ordered within the co-crystals. The C_{60} molecule is located at the 2a Wyckoff position for 2/m symmetry, whereas the solvent molecule is located at the 4h Wyckoff position (0, y=0.2768(2), 1/2). The two halogen atoms (Cl and Br) are statistically disordered with a 50/50 % distribution over their respective sites. For the low-temperature phase of $CBrClH_2$ the halogen atoms, Cl and Br, are also disordered with similar 0.5 occupancies as it was

reported for the low-temperature phase of $CBrClH_2$. The final Rietveld refinement yielded profile factors of Rwp=5.26% and Rp=3.83%, an overall isotropic temperature factor of 0.064 ± 0.001 and March-Dollase preferred orientation parameters of a*=-0.199(19), b*=-0.746(24), c*=0.636(26), Ro=0.917(6).

The stacking of alternating C_{60} and $CBrClH_2$ molecules is presented in Fig. 3. The solvent molecules have their 2-fold axis along the monoclinic axis b and the halogen ligands pointing along the longer diagonal of the a-c plane.

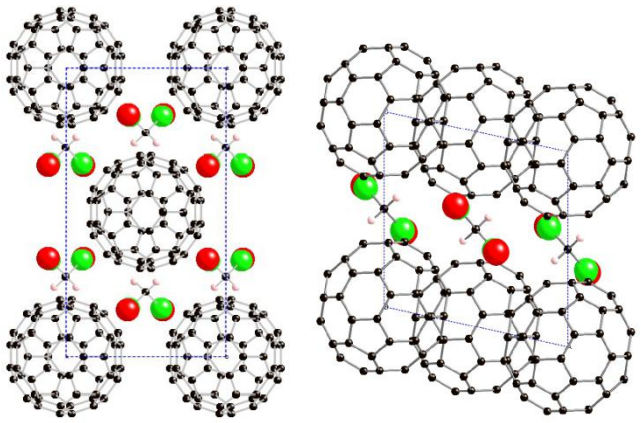

Fig. 3. The (001) plane (left panel) and the (010) plane (right panel) of the crystal structure of monoclinic C_{60}·$2CBrClH_2$ at 303 K. The overlap of the red (Br) and green (Cl) colored halogens highlight the occupational disorder.

To examine possible phase transitions, mixtures of co-crystals and their mother liquor were placed in stainless steel high-pressure pans for DSC studies and Lindemann capillaries to identify structural changes. The resulting DSC curve can be seen in Fig. 4. The endothermic peak P1 corresponds to the melting of excess monoclinic (C2/c) $CBrClH_2$ at virtually the same temperature as the pure solvent. [27] It corresponds to a degenerate eutectic equilibrium in the C_{60}-$CBrClH_2$ binary system. Peak P2, at 322 K, corresponds to a reversible solid-solid phase transition (see inset in Fig. 4a) without stoichiometric change of the co-crystal. As highlighted in Fig. 4b, the XRPD pattern at 333 K reveals a different structure for the co-crystal in relation to the one at 300 K. Preliminary DICVOL analysis revealed a hexagonal lattice with systematic absences compatible with the P6/mmm space group, isostructural to many other co-crystals of C_{60} with halogenated methane derivatives[14,16] and to the hexagonal phase of C_{60}.[28] The structure was analyzed using the FullProf Suite.[23] The C_{60} molecule was modeled with spherical harmonics describing a homogeneous distribution of 60 C-atoms located on a sphere of overall 3.59 Å radius. The center of C_{60} was positioned at the 1a Wyckoff position and the carbon of the tetrahedral $CBrClH_2$ molecule at the (1/3, 2/3, 1/2) position. The $CBrClH_2$ molecule was again described using a rigid body as for the low-temperature monoclinic structure. The C-atom position and orientation of the molecule were refined, obtaining a position of (0.329(6), 0.711(3), 0. 544(5)). The final Rietveld refinement yields profile factors of Rwp=4.02% and Rp=3.09%. Due to the fact that $CBrClH_2$ has a lower symmetry than that of the 2d site the resulting orientation of the molecule is in no special relation to the rotation axis and is therefore orientationally disordered. The refined and experimental patterns are depicted in Fig. 4b.

Finally, the DSC peak P3 at around 390 K in Fig. 4a shows the peritectic invariant (hexagonal C_{60}·$2CBrClH_2$ ⇔ liquid L +FCC C_{60}), i.e. the desolvation process of the hexagonal co-crystal. The phase diagram C_{60}: $CBrClH_2$ is shown in Fig. S1 (see Supp. Info).

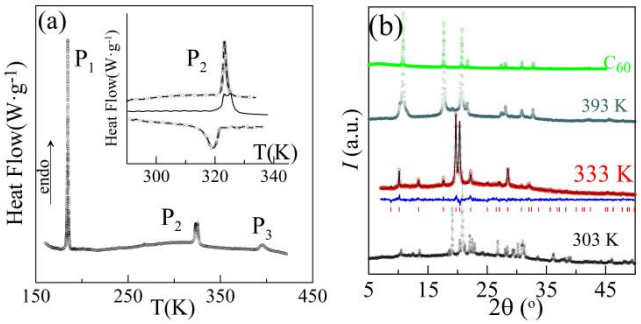

Fig. 4. (a) DSC curve of C_{60}·$2CBrClH_2$ in the presence of mother liquor obtained in a sealed pan. Peak P1 corresponds to the melting of $CBrClH_2$, peak P2 to the reversible order-disorder phase transition of C_{60}·$2CBrClH_2$ and peak P3 to the peritectic invariant (hexagonal C_{60}·$2CBrClH_2$ ⇔ L + FCC C_{60}). (b) XRPD patterns for C_{60}·$2CBrClH_2$ in the presence of mother liquor in a closed capillary as a function of temperature: 303 K, monoclinic solvate C_{60}·$2CBrClH_2$; 333 K, hexagonal solvate C_{60}·$2CBrClH_2$; 393 K, FCC C_{60} + liquid. The pattern at the top of the figure is that of fcc C_{60} and is provided for reference. For the pattern at 333 K the refinement results have been indicated as well: calculated pattern (black line), difference between calculated and experimental pattern (blue line) and the Bragg reflections (vertical red bars) of the hexagonal P6/mmm space-group of the C_{60}·$2CBrClH_2$ co-crystal obtained from the low-temperature monoclinic co-crystal by heating.

The order-disorder phase transition of the C_{60}·$2CBrClH_2$ co-crystal at around 322 K is accompanied with an enthalpy change of 4.85 $J{\cdot}g^{-1}$ (4.75(20) $kJ{\cdot}mol^{-1}$), as determined from the Tammann diagram of the solvent-rich side of the equilibrium involving the monoclinic and hexagonal forms of the solvate (see Fig. S2, Supp. Info). This enthalpy change involves an entropy change of 14.7(6) $J{\cdot}mol^{-1}K^{-1}$ which is of the same order as that involved in the order-disorder phase transition for the C_{60}·cubane co-crystal, in which similarly both C_{60} and cubane are orientationally frozen at low-temperature.[11,12] For C_{60} co-crystals with an order-disorder phase transition involving exclusively the solvent molecule, while C_{60} displays orientational disorder in both phases, the entropy change is about twice as small, 6.1 $kJ{\cdot}mol^{-1}K^{-1}$ for C_{60}·$2C(CH_3)Cl_3$ (at 212 K)[22] and 7.8 $kJ{\cdot}mol^{-1}K^{-1}$ for C60·$2CCl_4$ (at 223 K).[29] These thermodynamic values support the structural results reported.

Conclusions

The room temperature co-crystals C_{60}·$2CBrClH_2$ exhibit a monoclinic structure (space group C2/m), as revealed by X-ray powder diffraction, with both C_{60} and $CBrClH_2$ molecules orientationally ordered, the only disorder being that of the halogen atoms, Cl and Br, distributed over two sites with 0.5 occupancies. The structure displays stacking of alternating C_{60} and $CBrClH_2$ molecules with the solvent molecules having their

`

2-fold axis along the monoclinic axis b and the halogen ligands pointing along the longer diagonal of the a-c plane.
Without changing in stoichiometry, the co-crystal transforms at 322 K to a high-temperature hexagonal structure (space group P6/mmm) with similar packing to previously reported hexagonal co-crystals with halogen-methane derivatives.

Supporting Information

Crystallographic information files for monoclinic C_{60}·2CBrClH$_2$ at 303 K (C_{60}-2CBrClH$_2$-C2M.cif), and hexagonal C_{60}·2CBrClH$_2$ at 333 K (C_{60}-2CBrClH$_2$-P6MMM.cif).

Conflict of interest

The authors declare no competing financial interests.

Acknowledgements

This work has been supported by the Spanish MEC (FIS2017-82625-P) and by the Catalan government (2017SGR-42).

References

1 K. P. Meletov and G. A. Kourouklis, *JETP. Letters.*, 2012, **115**, 706-722.
2 B. Sundqvist, *Sci. Rep.*, 2014, **4**, 6171.
3 M. Yao, W. Cui, M. Du, J. Xiao, X. Yang, S. Liu, R. Liu, F. Wang, T. Cui, B. Sundqvist, B and Liu, *Adv. Mater.*, 2015, **17**, 3962-3968.
4 B. Tian, X. Zheng, T. J. Kempa, Y. Fang, N. Yu, G. Yu, J. Huang and C. M. Lieber, *Nature*, 2007, **449**, 885-889
5 S. S. Badu, H. Möhwald and T. Nakanishi, Chem. Soc. Rev., 2010, **39**, 4021-4035.
6 M. Sathish, K. Miyazawa, J. P. Hill and K. Ariga, *J. Am. Chem. Soc.*, 2009, **131**, 6372–6373.
7 J. J. Richards, A. H. Rice, R. D. Nelson, F. S. Kim, S. A. Jenekhe, C. K. Luscombe and D. C. Pozzo, *Adv. Funct. Mater.*, 2013, **23**, 514-522.
8 L. Wang, B. Liu, H. Li, W. Yang, Y. Ding, S. V. Sinogeikin, M. Yue, Z. Liu, X. C. Zeng, W. L. Mao, *Science*. 2012, **337**, 825-828.
9 R. Macovez, *Frontiers in Materials,* 2018, **4**, 46.
10 M. Yao, W. Cui, J. Xiao, S. Chen, J. Cui, R. Liu, T. Cui, B. Zou, B. Liu, and B. Sundqvist, *Appl. Phys. Lett.*, 2013, **103**, 071913.
11 S. Pekker, É. Kováts, G. Oszlányi, G. Bényei, G. Klupp, G. Bortel, I. Jalsovszky, E. Jakab, F. Borondics, K. Kamarás, M. Bokor, G. Kriza, K. Tompa and G. Faigel, *Nat. Mater.*, 2005, **4**, 764–767.
12 N. M. Nemes, M. García-Hernández, G. Bortel, É. Kováts, B. J. Nagy, I. Jalsovszky and S. Pekker, *J. Phys. Chem. B.*, 2009, **113**, 2042–2049.
13 J. Ye, M. Barrio, Ph. Negrier, N. Qureshi, I. B. Rietveld, R. Céolin and J. Ll. Tamarit, *Eur. Phys. J. Spec. Top.*, 2017, **226**, 857–867.
14 J. Ye, M. Barrio, R. Céolin, N. Qureshi, I. B. Rietveld, J. Ll. Tamarit, *Chem. Phys.*, 2016, 477, 39-45.
15 E. Mitsari, M. Romanini, N. Qureshi, J. Ll. Tamarit, M. Barrio, R. Macovez, *J. Phys. Chem. C.*, 2016, **120**, 12831–12839.
16 R. Céolin, D. O. López, B. Nicolaï P. Espeau, M. Barrio, H. Allouchi, J. Ll. Tamarit, *Chem. Phys.*, 2007, **342**, 78-84.
17 R. Céolin, J. Ll. Tamarit, M. Barrio, D.O. López, S. Toscani, H. Allouchi, V. Agafonov, and H. Szwarc. *Chem. Mater.*, 2001, **13**, 1349-1355.
18 F. Michaud, M. Barrio, S. Toscani, D.O. López, J.Ll. Tamarit, V. Agafonov, H. Szwarc and R. Céolin, *Phys. Rev. B.*, 1998, **57**, 10351-10358.
19 S. Toscani, H. Allouchi, J.Ll. Tamarit, D.O. López, M. Barrio, V.; Rassat, A. Agafonov, H. Szwarc and R. Céolin, Chem. Phys. Lett., 2000, **330**, 491-496.
20 F. Michaud, M. Barrio, D. O. Lopez, J. Ll. Tamarit, V. Agafonov, S. Toscani, H. Szwarc, and R. Céolin, *Chem. Mater.*, 2000, **12**, 3595-3602.
21 M. Barrio, D. O. López, J. Ll. Tamarit, P. Espeau and R. Céolin, *Chem. Mater.*, 2003, **15**, 288-291.
22 R. Céolin, J. Ll. Tamarit, M. Barrio, D. O. López, P. Espeau, H. Allouchi, and R. J. Papoular, *Carbon.*, 2005, **43**, 417-424.
23 J. Rodriguez-Carvajal, T. Roisnel and J. Gonzales-Platas, FullProf suite (2005 version). CEA-CNRS, CEN Saclay, France: Laboratoire Léon Brillouin, 2005.
24 MS Modeling (Materials Studio) version 5.5, http://www.accelrys.com /mstudio/ms_modeling.
25 M. Podsiadło, A. Katrusiak, *Acta Crystallogr., Sect. B.*, 2007, **63**, 903-911.
26 W. A. Dollase, *J. Appl. Crystallogr.*, 1986, **19**, 267-272.
27 C. L. Yaws, Thermophysical Properties of Chemicals and Hydrocarbons, 2nd Edition, 2014, 497.
28 R. Céolin, J. Ll. Tamarit, D. O. López, M. Barrio, V. Agafonov, H. Alluchi, F. Mussa and H. Szwarc. *Chem. Phys. Lett.*, 1999, **314**, 21-26.
29 M. Barrio, D. O. Lopez, J. Ll. Tamarit, H. Szwarc, S. Toscani and R. Céolin, *Chem. Phys. Lett.*, 1996, **260**, 78-81.